Pyk2 regulates cell-edge protrusion dynamics by interacting with Crk

Nikola Lukic[1], Stefanie Lapetina[1], Hanna Grobe[2], Kolluru D. Srikanth[1], Shams Twafra[1], Jonathan Solomon[1], Tal Sneh[1], Michal Gendler[1], Ronen Zaidel-Bar[2], and Hava Gil-Henn[1,*]

[1] Laboratory for Cell Migration and Invasion, The Azrieli Faculty of Medicine, Bar-Ilan University, Safed 1311502, Israel.

[2] Department of Cell and Developmental Biology, Faculty of Medicine, Tel-Aviv University, Tel-Aviv 69978, Israel.

* Correspondence should be addressed to: Hava Gil-Henn, The Azrieli Faculty of Medicine, Bar-Ilan University, 8th Henrietta Szold Street, P.O. Box 1589, Safed 1311502, Israel. Phone: +972-72-2644978, Fax: +972-72-2644978, e-mail: Hava.Henn@biu.ac.il

Running title: Pyk2-Crk interaction regulates protrusions

Abbreviations: Pyk2, protein tyrosine kinase 2; FAK, focal adhesion kinase; Crk, CT10 regulator of a tyrosine kinase; SH2, Src Homology 2; SH3, Src Homology 3; GFP, green fluorescent protein; YFP, yellow fluorescent protein; MEFs, mouse embryonic fibroblasts; WT, wild-type.

ABSTRACT

Focal adhesion kinase (FAK) is well established as a regulator of cell migration, but whether and how the closely related proline-rich tyrosine kinase 2 (Pyk2) regulates fibroblast motility is still under debate. Using mouse embryonic fibroblasts (MEFs) from $Pyk2^{-/-}$ mice, we show here, for the first time, that lack of Pyk2 significantly impairs both random and directed fibroblast motility. $Pyk2^{-/-}$ MEFs show reduced cell-edge protrusion dynamics, which is dependent on both the kinase and protein-protein binding activities of Pyk2. Using bioinformatics analysis of *in vitro* high-throughput screens followed by text mining, we identified CrkI/II as novel substrates and interactors of Pyk2. Knockdown of CrkI/II shows altered dynamics of cell-edge protrusions, which is similar to the phenotype observed in $Pyk2^{-/-}$ MEFs. Moreover, epistasis experiments suggest that Pyk2 regulates the dynamics of cell-edge protrusions via direct and indirect interactions with Crk which enable both activation and down-regulation of Crk-mediated cytoskeletal signaling. This complex mechanism may enable fine-tuning of cell-edge protrusion dynamics and consequent cell migration on the one hand together with tight regulation of cell motility, a process that should be strictly limited to specific time and context in normal cells, on the other hand.

INTRODUCTION

Cell migration is an evolutionary conserved process that controls the development and function of organisms and takes place in both normal as well as pathological processes, including embryogenesis, wound healing, immune response, angiogenesis, and cancer metastasis. Despite the differences in cell types that use migratory processes, it is believed that all mesenchymal cell motility events on two-dimensional adhesive substrates occur by similar molecular mechanisms and conserved signaling components (Kurosaka and Kashina, 2008). It is generally convenient to define cell migration into several component processes, which are often regulated by the same effectors regardless of the cell type and the mode of migration. The first stage in migration is polarization, in which the cell alters its biochemical and structural anatomy to have a distinct, stable front and rear as a response to directional cue from the extracellular environment. A polarized cell will then protrude by inducing actin polymerization at the leading edge of the cell that pushes the plasma membrane forward. The plasma membrane becomes attached to the substrate by anchoring actin bundles at the leading edge to focal adhesions and integrins. After the forward attachments have been made, the bulk contents of the cell body including the nucleus and other organelles translocate forward by myosin-dependent cortical contraction at the rear of the cell. At the last stage of migration, focal adhesions at the rear of the cell are broken, integrins are recycled, and the tail detaches by contraction of stress fibers or elastic tension and moves forward. These events are coordinated and integrated by extensive transient signaling networks which are initiated by the extracellular matrix, soluble factors, physical forces, or by neighboring cells (Ananthakrishnan and Ehrlicher, 2007).

The focal adhesion kinase (FAK) and its homologous FAK-related proline-rich tyrosine kinase 2 (Pyk2) are uniquely situated to act as critical mediators of integrin signaling and cell motility. While the role of FAK in regulation of cellular migration is well established, little is known about the contribution of the closely related Pyk2 to this process. Early publications suggested an increase in Pyk2 protein expression levels in $FAK^{-/-}$ MEFs (Sieg *et al.*, 1998; Lim *et al.*, 2008). Elevated Pyk2 expression levels are not sufficient to overcome the cell migratory defect in $FAK^{-/-}$ MEFs due to perinuclear localization of Pyk2 in these cells (Klingbeil *et al.*, 2001). Accordingly, chimeric proteins in which the FAT domain of Pyk2 was replaced with FAK-FAT domain showed localization to focal adhesions and rescue of the migratory defect of $FAK^{-/-}$ MEFs (Klingbeil *et al.*, 2001; Tomar *et al.*, 2009). While the role of Pyk2 in fibroblast motility and its ability to compensate for FAK have been elusive, a role for Pyk2 in regulation of cell migration in non-fibroblast cells has been firmly established. $Pyk2^{-/-}$ macrophages show significantly reduced cell motility which results from defects in cell polarization and actin polymerization, leading to

delayed leading edge lamellipodia formation and reduced detachment of their trailing edge (Okigaki *et al.*, 2003). Primary keratinocytes from Pyk2$^{-/-}$ show decreased MMP-dependent scratch wound repair *in vitro* and delayed skin wound healing in Pyk2$^{-/-}$ mice (Koppel *et al.*, 2014). A direct cell motility defect has also been demonstrated in Pyk2 knockdown triple negative breast cancer cells, which show significantly reduced random and directed cell migration *in vitro* (Genna *et al.*, 2018).

The CT10 regulator of a tyrosine kinase (Crk) family of adaptor proteins, which comprises of CrkI, CrkII, and the paralog CrkL, defines a novel class of regulatory adaptor proteins that act as major convergence points in tyrosine kinase signaling by physically bridging tyrosine phosphorylated proteins to various intracellular signaling pathways. The Crk proteins have central roles in a vast number of biological processes, ranging from cell proliferation, cellular adhesion and migration, phagocytic and endocytic pathways, apoptosis, and gene expression. The Crk adaptor proteins are composed of modular Src Homology 2 (SH2) and two Src Homology 3 (SH3) domains separated by flexible linker sequences, that act as building blocks to assemble multi-protein complexes. Both CrkII and CrkL are negatively regulated by tyrosine phosphorylation events that ultimately block their ability to function as adaptor proteins. Specifically, phosphorylation of CrkII on Tyr221 (Tyr207 on CrkL) causes intra-molecular binding of the linker region to the SH2 domain, sequestering the SH2 and SH3N and preventing them from binding target proteins (Birge *et al.*, 2009). This inhibitory phosphorylation of Crk proteins is mediated by the non-receptor tyrosine kinases Abl and Arg and is important for focal adhesion turnover and dorsal wave progression in fibroblasts (Antoku *et al.*, 2008; Antoku and Mayer, 2009). Unlike CrkII and CrkL, CrkI is missing the regulatory tyrosine residue and the C-terminal SH3 domain, and is therefore believed to be locked in a constitutively active conformation, that may also explain its high transforming capability. Crk proteins are involved in fibroblast cell spreading and migration, where they regulate signaling pathways leading to lamellipodia and filopodia formation and focal adhesion complex formation and turnover (Antoku *et al.*, 2008; Antoku and Mayer, 2009).

Our current study aimed to elucidate whether and how Pyk2 regulates fibroblast migration. We show here, for the first time, that a complete knockout of Pyk2 significantly reduced both random and directed cell motility in fibroblasts, which was correlated with impaired cell-edge protrusion dynamics in these cells. Interestingly, both the kinase and protein-protein binding activities of Pyk2 are essential for its ability to regulate the dynamics of cell-edge protrusions. Analysis of Pyk2 interacting proteins combined with text mining revealed CrkI/II as novel mediators of Pyk2 signaling in cell-edge protrusions. Indeed, Pyk2 directly binds and phosphorylates CrkII *in vitro*, and depletion of CrkI/II from MEFs results in a significant decrease in cell-edge protrusion dynamics, similar to the phenotype that was observed in Pyk2$^{-/-}$ MEFs. Epistasis experiments demonstrated that while overexpression of Pyk2 cannot compensate for the

loss of CrkI/II, expression of constitutively active CrkI or CrkII can completely rescue protrusion dynamics in Pyk2$^{-/-}$ MEFs. These data further suggest that CrkI/II proteins work downstream of Pyk2 to regulate cell-edge protrusion dynamics in fibroblasts. Pyk2 co-localizes with CrkII to focal adhesions, where it regulates their number and size and consequently the stabilization of protrusions at the cell edge.

Collectively, our findings identify Pyk2 as a unique mediator of cell-edge protrusion dynamics and cellular migration and provide a novel insight into the mechanism of Pyk2-mediated protrusion dynamics regulation.

RESULTS

Knockout of Pyk2 significantly reduces random and directed cell motility.

To explore the role of Pyk2 in fibroblast cell motility, we used immortalized mouse embryonic fibroblasts (MEFs) that were generated from embryos of wild-type (WT) and Pyk2$^{-/-}$ mice. Western blot analysis revealed high expression of Pyk2 in WT MEFs and complete deletion of Pyk2 in the knockout fibroblasts. Moreover, no differences in expression of the closely related FAK were observed in Pyk2$^{-/-}$ MEFs compared with their WT controls (Figure 1A).

To measure the invasion ability of Pyk2$^{-/-}$ MEFs as a group of cells, we used xCELLigence, which provides quantitative kinetic data of cell motility in real time. WT and Pyk2$^{-/-}$ MEFs were plated in serum starvation medium at the top chamber of an xCELLigence plate and their ability to invade through the pores towards a bottom chamber containing complete medium was examined over 24 hours. As demonstrated in Figure 1B-C, the ability of Pyk2$^{-/-}$ fibroblasts to invade into the lower chamber as a group over a period of 24 hours was significantly reduced (WT MEF, slope 1.166 ± 0.08; Pyk2$^{-/-}$ MEF, slope 0.356 ± 0.19).

To examine the ability of single cells to migrate in two-dimension (2D), WT or Pyk2$^{-/-}$ MEFs were plated on fibronectin and allowed to randomly migrate over it. As demonstrated in Figure 2A-D and Supplementary Movies S1-S2, Pyk2$^{-/-}$ MEFs showed significant decrease in migration velocity, in the total distance travelled (accumulated distance), and in Euclidean distance (the shortest distance between the starting and end points of migration), which is indicative of motility persistence and directionality.

To further evaluate the ability of Pyk2$^{-/-}$ fibroblasts to conduct directed and persistent cell motility towards a chemotactic gradient, we plated cells in a chemotactic chamber and measured their ability to migrate as single cells towards a serum gradient. As demonstrated in Figure 2E-H, features of directional cell motility such as directionality (straightness of cell movement), Y-forward migration index (cell path via the Y-axis only), and center of mass displacement (direction of movement of the group of cells) were significantly reduced in Pyk2$^{-/-}$ MEFs. Moreover, the

Rayleigh scattering test (final distribution of cells) was significant in WT MEFs only (WT, $p = 1.59e^{-08}$; Pyk2$^{-/-}$, $p = 0.26$), implying that these cells, as opposed to Pyk2$^{-/-}$ fibroblasts, move persistently towards one direction and not randomly as the Pyk2-deficient fibroblasts. Together, our data suggest that lack of Pyk2 in MEFs significantly affects different attributes of random and directed cell motility.

Pyk2$^{-/-}$ MEFs show reduced cell-edge protrusion dynamics.

During adhesion and spreading on fibronectin-coated surfaces, fibroblasts exhibit frequent dynamic protrusions and retractions of the cell-edge, which are reminiscent of the leading-edge protrusions in a migrating cell. These dynamic cell-edge protrusions are both a prerequisite and a rate-limiting step in cell motility and are controlled by mechanisms which are highly relevant to cell migration, such as actin polymerization, myosin-mediated contractility, and focal adhesion turnover.

To evaluate a role of Pyk2 in cell-edge protrusion dynamics, we analyzed time-lapse movies of WT and Pyk2$^{-/-}$ fibroblasts by kymography (Hinz *et al.*, 1999), which represents a timeline of protrusion and allows quantitation of several parameters, such as protrusions (cell-edge membrane extensions driven by actin polymerization which pushes the plasma membrane forward), retractions (derived by contractile forces at the cell-edge and anterior lamella), and ruffles, which represent protrusions that fail to attach to the growth substrate during migration. As shown in Figure 3A-E and Supplementary Movies S3-4, knockout of Pyk2 significantly reduced the frequencies of protrusions, retractions, and membrane ruffles, suggesting that Pyk2 regulates the dynamics of cell-edge protrusions by controlling one or more of these attributes.

Regulation of cell-edge protrusion dynamics in fibroblasts depends on both the kinase and binding activities of Pyk2.

To determine whether regulation of cell-edge protrusion dynamics is mediated by the kinase activity of Pyk2 or by binding to its effectors, we re-expressed GFP-tagged Pyk2 kinase inactive mutant (Pyk2-KI-GFP), an autophosphorylation and Src-binding mutant of Pyk2 (Pyk2-Y402F-GFP), or a mutant in the second (Pyk2-PRR2-GFP) or third (Pyk2-PRR3-GFP) proline-rich regions of Pyk2, which mediate binding of Pyk2 to downstream signaling proteins, in Pyk2$^{-/-}$ cells in expression levels which were similar to endogenous Pyk2 in WT MEFs (Figure 4A-B). Interestingly, re-expression of WT-Pyk2-GFP significantly increased the frequencies of protrusions, retractions, and ruffles to levels similar to WT cells. None of the Pyk2 mutants rescued cell-edge protrusion dynamics attributes to levels similar to Pyk2$^{-/-}$ re-expressing WT-Pyk2-GFP (Figure 4C-K and Supplementary Movies S5-S10), suggesting that both the kinase activity and protein-protein binding are essential for regulation of the dynamics of cell-edge protrusions by Pyk2.

CrkII is a potential substrate and interactor of Pyk2 in cell-edge protrusions.

To gain insight into the molecular mechanisms and signaling pathways by which Pyk2 regulates cell-edge protrusion dynamics, we examined the data of high-throughput protein-protein and kinase-substrate protein microarrays that were previously performed in our laboratory using purified Pyk2 as a bait (Genna *et al.*, 2018). The lists of proteins from these screens were overlaid with a list of proteins that was generated by literature mining using the term "cell-edge protrusions" (Supplementary Table S1). Overlay of protein-protein interaction list with cell-edge protrusions revealed five proteins, CrkI, CrkII, cortactin (CTTN), NCK1, and BAIAP2. Overlay of the kinase-substrate interaction list with cell-edge protrusions revealed only three proteins, CrkI, CrkII, and cortactin. Interestingly, overlay of both protein-protein interaction and kinase-substrate interaction lists with cell-edge protrusion list revealed CrkI, CrkII, and cortactin as cell-edge protrusion-related candidate proteins that are both direct substrates and interactors of Pyk2 (Figure 5A). While direct interaction between Pyk2 and cortactin has previously been demonstrated in invadopodia (Genna *et al.*, 2018), database search using STRING followed by manual literature validation using PubMed identified CrkI/II as novel and direct substrates and interactors of Pyk2. Values of Pyk2-CrkI/II protein-protein and kinase-substrate interactions that were detected in our previous protein microarray screens are shown in Figure 5B-C.

Pyk2 directly binds and phosphorylates CrkII.

To validate that Pyk2 binds CrkII directly, we performed the *in vitro* pulldown assay (Lapetina and Gil-Henn, 2017) using purified Pyk2 and CrkII. Increasing concentrations of purified WT-CrkII, CrkSH2 (R38K; mutation at the N-terminal SH2 domain), CrkNSH3 (W169K; mutation at the N-terminal SH3 domain), or CrkCSH3 (W276K; mutation at the C-terminal SH3 domain) (Figure 6H) were incubated with constant concentration of Pyk2, and the amounts of bound CrkII were quantified. As shown in Figure 6A-B, WT-CrkII binds to Pyk2 with a K_d of 0.150 ± 0.03 μM, CrkSH2 mutant bound Pyk2 with a higher K_d of 0.508 ± 0.158 μM (Figure 6 C-D), a mutant of CrkII at its C-terminal SH3, which is considered as a pseudo SH3 domain, bound Pyk2 in a K_d of 0.134 ± 0.034 μM (Figure 6E-F), while no binding of CrkII mutated in its N-terminal SH3 (CrkNSH3; W276K) was observed (Figure 6G), suggesting that CrkII binds directly to Pyk2 via its N-terminal SH3 domain. To examine whether Pyk2 can directly phosphorylate CrkII, we performed the *in vitro* kinase assay using purified recombinant Pyk2 and either WT-CrkII or a tyrosine phosphorylation-deficient mutant of CrkII (CrkII-Y221F) (Figure 7A). As shown in Figure 7B-E, Pyk2 directly phosphorylated WT-CrkII (K_M = 0.287 ± 0.05 μM, k_{cat} = 0.057 ± 0.008 μM/min), while no phosphorylation of CrkII-Y221F was observed (Figure 7E), suggesting that Pyk2 directly

phosphorylates CrkII on its auto-inhibitory tyrosine 221. Overall, these data validate our protein arrays findings and suggest that Pyk2 directly binds and tyrosine phosphorylates CrkII.

Knockdown of CrkII shows significant alteration of cell-edge protrusion dynamics.

Crk proteins are well known in cell migration and cytoskeletal signaling ((Antoku *et al.*, 2008; Antoku and Mayer, 2009; Birge *et al.*, 2009; Park and Curran, 2014), however their specific role in cell-edge protrusion dynamics has not been documented before. To explore the potential involvement of CrkI and CrkII in cell-edge protrusion dynamics, we transiently knocked them down in WT MEFs using siRNA. Because CrkI is identical in sequence to CrkII and only missing the C-terminal SH3 domain, an siRNA sequence targets both proteins when used on WT MEFs but does not target the closely related CrkL (Figure 8A). Importantly, knockdown of CrkI/II in WT MEFs significantly reduced the frequencies of protrusions, retractions, and membrane ruffles (Figure 8B-F and Supplementary Movies S11-12), suggesting that similar to Pyk2, CrkI/II proteins regulate the dynamics of cell-edge protrusions by controlling one or more protrusion dynamics traits.

Pyk2 and CrkII coordinately regulate cell-edge protrusion dynamics.

The similarity between Pyk2 and CrkII in cell-edge protrusion dynamics phenotypes, together with the direct binding and phosphorylation of CrkII by Pyk2 suggest that the two proteins cooperate within the same signaling pathway in MEFs. To test this hypothesis, we used MEFs overexpressing Pyk2-GFP and treated with CrkI/II siRNA or a non-silencing siRNA. Cells that overexpressed Pyk2 and were treated with CrkI/II siRNA showed a significant reduction in frequencies of protrusions, retractions, and ruffles (Figure 9A-E), suggesting that overexpression of Pyk2 cannot compensate for CrkI/II depletion. We then tested whether expression of CrkII-Y221F-YFP or CrkI-YFP, two constitutively activated forms of Crk, can bypass the loss of Pyk2 in $Pyk2^{-/-}$ MEFs. Interestingly, either the CrkII-Y221F mutant or CrkI could bypass the loss of Pyk2 in $Pyk2^{-/-}$ MEFs and significantly increased protrusions, retractions, and ruffles when expressed in Pyk2-depleted cells (Figure 9F-K). The phenotype rescue by the CrkII-Y221F mutant or CrkI suggests that in absence of Pyk2, Crk proteins are recruited to the cell membrane by another protein, such as the closely related FAK. Indeed, Vuori K. *et al.* have previously shown a mechanism by which integrin-induced FAK activation in fibroblasts leads to p130Cas-mediated recruitment of CrkII and downstream cytoskeletal signaling (Vuori *et al.*, 1996). While FAK may compensate for recruitment of Crk proteins, this compensatory activity is not sufficient for overcoming the protrusion dynamics and migration defects of $Pyk2^{-/-}$ MEFs. Collectively, these results suggest that Crk may act downstream to Pyk2 in regulating cell-edge protrusion dynamics in fibroblasts.

Pyk2 co-localizes with CrkII at focal adhesions and regulates their number and size.

A potential mechanism by which Pyk2 regulates cell-edge protrusion dynamics and consequent cell motility is by controlling the formation or turnover of focal adhesions. To test this, we first examined the localization of Pyk2 in Pyk2$^{-/-}$ MEFs re-expressing fluorescently tagged WT-Pyk2 and labeled for vinculin as a focal adhesion marker. As shown in Figure 10A and Supplementary Movie S13, Pyk2 co-localizes with vinculin and paxillin to focal adhesions at the cell-edge.

Crk proteins are essential components of focal adhesions and are required for their formation and disassembly. Moreover, changes in tyrosine phosphorylation of Crk proteins correlate with the size and number of focal adhesions in cells (Antoku *et al.*, 2008; Antoku and Mayer, 2009). Indeed, fluorescent live imaging of CrkII demonstrated its localization to focal adhesions at the cell-edge together with vinculin (Supplementary Figure 1 and Supplementary Movie S14). Moreover, Pyk2 and CrkII co-localized to focal adhesions at the cell-edge of MEFs (Figure 10B, Supplementary Figure 1 and Supplementary Movie S15).

To test whether Pyk2 regulates focal adhesions, WT and Pyk2$^{-/-}$ MEFs were plated on fibronectin, fixed after 30 minutes, 1 hour, or three hours, and labeled for vinculin and actin, and their focal adhesions were quantified. Interestingly, while Pyk2$^{-/-}$ MEFs showed significantly fewer focal adhesions, their size was much larger than focal adhesions of WT fibroblasts (Figure 10C-F). These data may imply that Pyk2 regulates both the formation as well as turnover of focal adhesions. Together, these results suggest that Pyk2 regulates cell-edge protrusion dynamics and consequent cell migration by controlling focal adhesion formation and turnover at the cell-edge as well as other cytoskeletal mechanisms.

DISCUSSION

Since the characterization of FAK$^{-/-}$ phenotype in mouse embryonic fibroblasts (Ilic *et al.*, 1995), a role for the closely related Pyk2 in cell migration and its ability to compensate for FAK has been controversial. In this study, we aimed to determine whether and how Pyk2 regulates fibroblast motility using MEFs isolated from Pyk2 knockout mice. We demonstrate here, for the first time, that Pyk2$^{-/-}$ MEFs have severe impairment in random and directed cell motility, which correlates with significantly reduced dynamics of cell-edge protrusions and with severe impairment in focal adhesion regulation. We further uncover CrkII as a novel mediator of Pyk2 signaling and suggest a complex mechanism which enables dynamic regulation of cell-edge protrusions, which is both a prerequisite and a rate-limiting step for cell motility.

Pyk2 regulates fibroblast motility in a non-compensatory mechanism.

The role of Pyk2 in fibroblast motility and its ability to compensate for the closely related FAK in these cells has been under debate over the past two decades. Part of this controversy may have resulted from the use of cells in which a knockdown of Pyk2 was used, and where residual amounts of Pyk2 remain, which may lead to biased conclusions. In this study, we used a complete knockout system in which no Pyk2 expression is observed, to demonstrate a significant role of Pyk2 in regulation of cell motility. To our knowledge, this is the first documentation of the Pyk2 knockout phenotype in fibroblast migration and in protrusion dynamics regulation. Continuing the same line, previous publications using FAK knockout fibroblasts documented an increase in Pyk2 protein expression levels which fails to compensate the cell motility impairment in $FAK^{-/-}$ cells (Sieg *et al.*, 1998; Klingbeil *et al.*, 2001). Despite the constitutive depletion of Pyk2 in the cells used in our current study, no changes in FAK protein expression levels were observed in $Pyk2^{-/-}$ MEF. Moreover, the fact that we observed significant motility and protrusion dynamics phenotypes in the $Pyk2^{-/-}$ MEFs suggests no compensatory role of FAK over Pyk2 in Pyk2 knockout fibroblasts. This may also imply that Pyk2 and FAK use some overlapping but mainly distinct mechanisms to regulate protrusion dynamics and cell motility in fibroblasts.

Pyk2 controls cell-edge protrusion dynamics in a complex mechanism.

One of the early steps in cell migration is the formation of an actin polymerization-mediated membrane protrusion at the cell-edge, which determines the direction of cell movement. The dynamics of cell-edge protrusions at the leading edge is essential for proper cellular migration (Hinz *et al.*, 1999), and can be recapitulated and dissected in the cell-edge protrusion assay used in this study. The assay examines the frequency of protrusions, which are driven by actin polymerization at the cell-edge, retractions, which are mainly controlled by myosin II activity, and ruffles, which are indicative of focal adhesion dynamics. Close examination of the $Pyk2^{-/-}$ MEFs cell-edge protrusion phenotypes in this assay revealed significant reduction in the frequency of all three attributes. This may imply that Pyk2 regulates protrusion dynamics and related cell migration by a complex mechanism which combines several different cytoskeletal pathways and processes.

Cell movement initiates by the formation of actin polymerization-mediated leading-edge membrane protrusions which are stabilized by focal adhesions that anchor the protruding cell membrane to the ECM (Parsons *et al.*, 2010). Interestingly, Pyk2 was shown to regulate actin polymerization (Gil-Henn *et al.*, 2007; Roa-Espitia *et al.*, 2016), and localizes to focal adhesions (Litvak *et al.*, 2000; Genna *et al.*, 2018) in other cell types, suggesting it may have a role in these processes. We show here, for the first time, that Pyk2 co-localizes with CrkII to focal adhesions in

MEFs, where it regulates the number and size of these structures. Based on these findings, we suggest that Pyk2 regulates the dynamics of cell-edge protrusions and consequent cellular migration by controlling both actin polymerization, which generates the protrusions, as well as focal adhesion formation and turnover, which stabilize these protrusions at the cell-edge.

An integrated model for the role of Pyk2 in regulation of cell-edge protrusion dynamics.

Based on previous knowledge and on our data presented herein, we suggest the following model for Pyk2-Crk mediated regulation of cell-edge protrusion dynamics (Figure 11). Integrin binding stimulates Pyk2 autophosphorylation followed by recruitment and activation of Src, which leads to complete activation of Pyk2 by phosphorylating its kinase activation loop tyrosines. Activated Src further phosphorylates p130Cas, which recruits Crk and induces downstream signaling via DOCK180/ELMO-Rac1-WAVE-Arp2/3, leading to actin polymerization and consequent cel- edge protrusions. This complex also leads to the formation of focal adhesions which stabilize membrane protrusions at the cell-edge and regulate their dynamics. Activated Pyk2 can also bind directly to Crk and phosphorylate it on tyrosine 221, which leads to its autoinhibition and to downregulation of Crk-mediated signaling.

Our model suggests that Pyk2 regulates the dynamics of cell-edge protrusions via a complex mechanism which involves both direct and indirect interactions with Crk, and which enables both activation and amplification as well as down regulation of Crk-mediated cytoskeletal signaling. This suggested mechanism enables both fine-tuning of the dynamic traits of cell-edge protrusions as well as tight regulation of cell motility, that should be activated only at specific times and contexts in normal cells.

Pyk2 in fibroblast motility: physiological and pathological implications.

Fibroblasts play a significant role in wound repair, an essential physiological process that is important for tissue homeostasis. During normal wound healing, connective tissue is repaired exclusively through the action of fibroblasts, which migrate into the wound site where they synthesize and remodel new extracellular matrix (ECM), and generate the contractile force necessary for wound closure. The ability of these fibroblasts to migrate, attach to the ECM and remodel it is mediated by the activity of integrins and associated focal adhesion complexes. Moreover, impairment in migration or activity of these fibroblasts can lead to delayed wound healing, excessive scarring, or fibrotic disorders (Martin, 1997; Eckes *et al.*, 1999; Gurtner *et al.*, 2008). Hence, understanding the basic mechanisms of fibroblast migration and activity during

wound repair is essential for controlling normal tissue repair and may also lead to development of novel effective anti-fibrotic therapies.

The process of wound repair has been studied most extensively in the skin. Indeed, it was recently shown that Pyk2 regulates keratinocyte function and consequent *in vivo* wound healing by controlling PKCδ-mediated MMP expression and secretion. Wounds that were made in the skin of Pyk2 knockout mice healed significantly slower than wounds in control, WT mice (Koppel *et al.*, 2014). Because the mouse model used in this work was a complete Pyk2 knockout in which Pyk2 has been deleted in all tissues and cell types, the possibility that impaired wound closure in Pyk2 knockout mice *in vivo* may result from impairment in function of other cell types that take part in wound repair, such as fibroblasts, could not be completely ruled out. Our data presented herein suggest that fibroblasts isolated from $Pyk2^{-/-}$ mice have severe impairment in cell migration and may imply that they have a subsequent defect in wound healing *in vivo*. This potential role of Pyk2 in fibroblast-mediated wound repair is a subject for future investigation.

MATERIALS AND METHODS

Generation of $Pyk2^{-/-}$ MEFs

$Pyk2^{-/-}$ mice were generated as previously described (Okigaki *et al.*, 2003). Mouse embryonic fibroblasts were generated from 11.5-13.5 days old embryos of WT and $Pyk2^{-/-}$ mice. Cells from five different embryos from each genotype were pooled together and immortalized by infection with a retrovirus expressing SV40 large T antigen followed by selection with 4mM Histidinol for three weeks.

DNA constructs, RNAi, and transfection

Pyk2-WT-GFP, Pyk2-Y402F-GFP (auto-phosphorylation and Src SH2 domain binding site mutant), and Pyk2-K457A-GFP (kinase inactive mutant, KI) were generated by sub-cloning WT and mutant Pyk2 cDNAs (Gil-Henn *et al.*, 2007) into the pQCTK-GFP retroviral plasmid (a modified version of pQC plasmid, kindly provided by Dr. Anthony Koleske, Yale University, USA). Pyk2-PRR-GFP constructs containing mutations in proline-rich region 2 (PRR2; P714A, P717A, P720A) or proline-rich region 3 (PRR3; P856A, P859A) of Pyk2 were generated from pQCTK-Pyk2-WT-GFP by the Quickchange site directed mutagenesis kit (Agilent Technologies). RNAi-resistant pMCV-puro-YFP constracts for CrkI, CrkII, and CrkII-Y221F (Antoku and Mayer, 2009) were kindly provided by Dr. Bruce Mayer, University of Connecticut, USA. For siRNA-mediated knockdown of CrkI/II, control non-silencing siRNA SMARTpool (D-001810-10) and CrkI/II siRNA SMARTpool (L-061117-00) were obtained from Dharmacon. Transient transfection of siRNA and Crk constructs was performed using the nucleofection method. Briefly, $0.8x10^6$ cells

where trypsinized and washed with PBS. Cells were re-suspended in 100µl mix containing a 1:50 ratio of Solution 1 (20% ATP-disodium salt and 12% of $MgCl_2$) and Solution 2 (1.2% KH2PO4, 0.12% NaHCO3 and 0.04% glucose). Next, cells were mixed with 3µg plasmid DNA or 2µM siRNA and immediately electroporated using Nucleofector 2b device (Lonza), T-020 protocol. Cells were used for experiments 48 hours following plasmid transfection or 72 hours following siRNA transfection.

Cell line generation

Stable cell lines expressing Pyk2-WT-GFP, and GFP-tagged mutants of Pyk2 were generated by co-transfecting pQCTK-Pyk2-GFP and pVSVG plasmids into GP2 packaging cells. Viral sups were used to infect MEFs, which were then selected with 100 µg/ml Hygromycin. Expression levels were verified by western blot analysis. A control cell line was generated by infection with viral sups containing pQCTK-GFP.

Reagents and antibodies

Fibronectin from human plasma (F0895) and L-Histidinol Dihydrochloride (H6647) were obtained from Sigma-Aldrich. Hygromycin (#ant-hg) was obtained from InvivoGen. For western blot, anti-Pyk2 (3292) was obtained from Cell Signaling Technology; anti-FAK (610088) and anti CrkI/II (610036) were obtained from BD Transduction Laboratories; anti-CrkL (sc-319) was obtained from Santa Cruz Biotechnology; anti-GFP (11814460001) was obtained from Roche Life Science; anti-β-actin (clone AC-15) (A5441) was obtained from Sigma-Aldrich; anti-HSC-70 (1427) was obtained from Abcam. Secondary antibodies (goat anti-mouse 680LT and goat anti-rabbit 800CW) were obtained from LI-COR Biosciences. For immunofluorescence, anti-vinculin (V9131) was obtained from Sigma-Aldrich; Rhodamine-labelled phalloidin and Alexa Fluor-conjugated secondary antibodies were obtained from Molecular Probes.

Western blot analysis

Cells were washed twice in ice cold PBS and lysed in modified radio-immunoprecipitation assay (mRIPA) buffer (50 mM Tris, pH 7.2, 150 mM NaCl, 1% NP-40, 0.5% deoxycholate, 0.1 %SDS, 1 mM EDTA, 2 mM NaF, 1 mM Na_3VO_4, and protease inhibitors). Total protein concentration was determined using DC Protein Assay (Bio-Rad) and equal amounts were loaded on SDS-PAGE, transferred to a nitrocellulose membrane, blocked in Odyssey blocking buffer, incubated with primary antibodies and secondary antibodies, and imaged using the Odyssey® CLx imaging system (LI-COR Biosciences).

Single cell random migration assay

µ-slide 8 well chambered coverslips (ibidi) were coated with 10 µg/ml fibronectin and blocked with 1% BSA. 20,000 cells were plated in each well in DMEM/10% FBS and allowed to adhere for 3 hours. Before imaging, medium was replaced by DMEM/10% FBS/10 mM HEPES. Cells were placed in a 37°C heated chamber and images were collected using the Leica AF6000 inverted microscope (40x, NA 0.60, air objective). Phase images were acquired every 5 minutes for eight hours. Trajectory plots, velocity (rate of change in cell position as a function of time), accumulated distance (total distance travelled), Euclidean distance (the shortest distance between the starting and end points of migration), directness (a measure of the straightness of the cell trajectories, calculated by comparing the Euclidean distance and the accumulated distance between the starting point and end point of a migrating cell), forward migration index (the efficiency of the forward migration of cells), center of mass displacement (the average of all single cell endpoints, indicates the direction in which the group of cells travelled), and Rayleigh test (statistical test for the uniformity of a circular distribution of cell endpoints) were calculated using the chemotaxis and migration tool (ibidi).

Directional migration assay

2,000 cells were plated in the central arena of 1µm µ-slide chemotaxis apparatus (ibidi). In the upper compartment DMEM/10% FBS was applied, and DMEM/0.5% FBS was applied in the bottom compartment. Cells were allowed to adhere for three hours and then placed in a 37°C heated chamber and images were collected using the Leica AF6000 inverted microscope (40x, NA 0.60, air objective). Phase images were acquired every 10 minutes for eight hours. Cell trajectories were obtained using Fiji with the "Track cell" command. Trajectory plots, accumulated distance, Euclidean distance, velocity, directness (mathematical representation of cell path towards chemoattractant), Y-forward migration index (cell path via the Y axis only), center of mass displacement (movement of the group of cells), and Rayleigh scattering test (final dispersion of cells) were calculated using the chemotaxis and migration tool (ibidi).

Chemotactic motility assay

The invasion ability of cells was measured using the xCELLigence RTCA DP instrument (Acea Biosciences), which measures electrical cell impedance that is directly correlated with the number of cells that pass from the upper to the lower chamber through the pores. 40,000 cells were serum starved overnight and plated in the upper chamber of CIM plate 16 platform containing serum-free medium, while the lower chamber was filled with DMEM/10% FBS. After initial measurement of

baseline impedance cells were left to adhere for 3 hours. Subsequently impedance was measured every 15 minutes for 24 hours.

Cell-edge protrusion dynamics assay

The cell-edge protrusion dynamics assay was performed as previously described (Lapetina *et al.*, 2009; Miller *et al.*, 2010). Briefly, 20,000 cells were plated on 10 µg/ml fibronectin-coated glass bottom dish that was blocked with 1% BSA and allowed to attach and spread for 15 minutes at 37^0 C, 5% CO_2. Plates were then placed in a 37°C heated chamber and images were collected using the Leica AF6000 inverted microscope (40x, NA 0.60, air objective). Phase images were acquired every 5 seconds for 10 minutes. Kymographs of cell membrane were obtained using Fiji with the "Reslice" command, and manually analyzed for protrusions, retractions and ruffles.

Protein purification

His-tagged Pyk2 was expressed and purified from High Five cells as previously described (Genna *et al.*, 2018). GST-tagged CrkII construct for expression of recombinant chicken CrkII in bacteria was kindly provided by Dr. Bruce Mayer, University of Connecticut, USA. The CrkII mutants R38K (CrkSH2; mutation at the N-terminal SH2 domain), W170K (CrkNSH3; mutation at the N-terminal SH3 domain), W276K (CrkCSH3; mutation at the C-terminal SH3 domain), and Y222F (tyrosine phosphorylation site mutant) were generated by site-directed mutagenesis.
GST-CrkII was expressed in *Escherichia coli* using 0.5 mM IPTG and overnight incubation at 27°C. Bacteria were lysed at 4°C in lysis buffer (PBS with 10 mM EDTA, 1mM PMSF, and protease inhibitors) using French press. 10% Triton was then added to the lysate, and the lysate was incubated on ice for 10 minutes. The lysate was clarified by centrifugation at 12,000 rpm for 20 minutes, and then purified over a glutathione agarose column using glutathione elution buffer (10mM glutathione in PBS and protease inhibitors) to elute. Peak fractions were pooled and dialyzed against dialysis buffer (20mM HEPES pH 7.25, 100mM KCl, 0.01% NP40, 500 mM DTT, 5% glycerol, and protease inhibitors).

Quantitative *in vitro* binding assay

Quantitative *in vitro* binding assay was performed as previously described (Lapetina and Gil-Henn, 2017). Briefly, purified Pyk2 was buffer exchanged into 3.65X PBS buffer using a G-25 Sephadex column by gravity flow and covalently coupled to AminoLink beads (Thermo Scientific) according to the manufacturer's instructions to a final concentration of 1 mM. The remaining active sites on

protein-linked beads were blocked in 1M Tris-HCl pH 7.25, 100 mg/ml BSA. Recombinant GST-CrkII was buffer exchanged into binding buffer (25 mM HEPES buffer pH 7.25, 100 mM NaCl, 0.01% Triton, 5% Glycerol, and 1 mM DTT) using a G-25 Sephadex column. 490 µl of serial dilutions of GST-CrkII (0-5 µM) were incubated with 10 µl of 1mM Pyk2-linked beads or 10 µl of BSA control beads for 1 hour at 4°C with rotation. Following incubation, the supernatant was removed, beads were briefly washed, bound material was recovered by boiling in Laemmli sample buffer and separated on 10% SDS-PAGE. Gel bands were resolved using Coomassie blue silver stain, and their densities were quantified using ImageJ software. For measurements of binding affinities (K_d), band densities were plotted against concentration of the free solution protein, and binding isotherms were set using the GraphPad Prism software using the one site-specific binding equation: $Y = B_{max} \times X/(X+K_d)$. In this equation, Y equals the specific binding signal, X equals the concentration of CrkII added to Pyk2 beads, and B_{max} is the maximum specific binding. The equilibrium constant K_d is solved as the value of X when Y equals 50% of B_{max}. To ensure saturation of the curves, CrkII maximal concentrations of at least five times the K_d were used in the assay.

***In vitro* kinase assay**

Purified Pyk2 (10 nM) was pre-incubated with increasing concentrations of CrkII (0-2 µM) for 5 minutes at 32°C. The reactions were started by addition of 5 µM cold ATP and 0.75 µCi of radiolabeled γ^{32}P-ATP (Perkin Elmer, BLU502H) in kinase buffer (25 mM HEPES, 100 mM NaCl, 5% Glycerol, 5 mM $MgCl_2$, 5 mM $MnCl_2$, 1 mM Na_3VO_4, 1 mM DTT) and incubated at 32^0C for additional 5 minutes. All reactions were quenched with Laemmli sample buffer, boiled, and separated on 10% SDS-PAGE. The gels were exposed to a phosphorimaging screen overnight, scanned using a Personal Molecular Imager (Bio-Rad), and band densities were quantified using the Quantity One software (BioRad). The values for each concentration series were analyzed by GraphPad software and fitted to Michaelis-Menten isotherms, $Y = V_{max}*X/(K_M+X)$, where Y is the enzyme velocity, V_{max} is the maximum enzyme velocity, X is the substrate concentration, and K_m is the substrate concentration needed to achieve a half-maximal enzyme velocity. Following exposure and phosphorimaging scanning, gels were stained with Coomassie blue silver to visualize cortactin bands. Specific and negative control bands were cut out of the gel and quantified by a scintillation counter along with 2 µl sample from the kinase assay. The number of counts per minute was calculated and corrected to integrated density from ImageJ software, and k_{cat} values were determined as previously described (Boyle and Koleske, 2007).

Immunofluorescence

WT or Pyk2$^{-/-}$ MEFs were plated on 10 μg/ml fibronectin-coated glass coverslips for 24 hours and fixed in 3.7% paraformaldehyde. Cells were permeabilized with 0.1% Triton X-100, blocked with 1% FBS and 1% BSA in PBS, and then labeled with anti-vinculin. Images were acquired using an inverted fluorescent microscope (AF6000; 63x 1.3 NA with oil objective with LAS AF acquisition software; Leica Microsystems) equipped with an ORCA-Flash 4.0 V2 digital CMOS camera (Hamamatsu Photonics). For images presented in Figure 10, imaging was performed using TIRF with 100X lens.

Focal adhesion quantification

WT or Pyk2$^{-/-}$ MEFs were plated on 10 μg/ml fibronectin-coated glass coverslips, fixed after 30 minutes, 1 hour, and 3 hours following plating, and labeled with anti-vinculin and Rhodamine-labeled phalloidin. Focal adhesions were quantified using Fiji and their average number and size were calculated and normalized to total cell size as follows:

Relative number of focal adhesions (A.U.) = focal adhesion number / cell size (μm^2)

Relative size of focal adhesions (A.U.) = focal adhesion size (μm^2) / cell size (μm^2)

Fluorescent live imaging

Cells were transfected using MirusLTI and imaged after 48 hours in a 24 well glass bottom plate. Plates were then placed in a 37^0 C heated chamber and images were collected using a Nikon Ti2E microscope (Plan APO 100x/1.4 NA oil immersion objective) equipped with Yokogawa W1 spinning disk system. For live cell imaging, images were captured at a single z-plane. Movies were prepared using Fiji.

Protein microarrays and text mining

Protein-protein and kinase-substrate protein microarrays were performed by Invitrogen as previously described (Genna *et al.*, 2018). Comparative text mining search was performed using Geneshot (Lachmann *et al.*, 2019) with the query "cell-edge protrusions". The lists of proteins identified by Geneshot (a total of 124 proteins; (Genna *et al.*, 2018)) and proteins identified in PPI and KSI ProtoArray screens (a total of 126 non-redundant proteins; (Genna *et al.*, 2018)) were used to build networks of physical and functional associations in STRING, and networks were overlaid using Cytoscape (Shannon *et al.*, 2003). Overlap between proteins from PPI, KSI, and cell-edge protrusions groups was determined using Venny 2.1.0 (Oliveros, 2015) and validated by manual literature search in PubMed.

Statistical analysis

Statistical analysis was performed using GraphPad Prism 8.0. Statistical significance was calculated using unpaired, two-tailed Student's *t*-test when two groups were compared, or ANOVA with Dunnett's posthoc test when three or more groups were compared. Values were considered statistically significant if the P value was ≤ 0.05. For all figures, * indicates P value ≤ 0.05; ** indicates P value ≤ 0.01; and *** indicates P value ≤ 0.001. Error bars represent the standard error of the mean (SEM).

ACKNOWLEDGEMENTS

This work was supported by grants from the Israel Science Foundation (grants number 1462/17 and 2142/21), the Israel Cancer Research Fund (grant number 20-101-PG), and the Israel Cancer Association (grant number 20210071) (to Hava Gil-Henn) and a grant from the Israel Science Foundation (grant number 3308/20) (to Ronen Zaidel-Bar). We wish to thank Dr. Anthony Koleske for his kind assistance and advice in the *in vitro* kinase and binding assays, and Dr. Bruce Mayer for his kind gift of Crk constructs.

REFERENCES

Ananthakrishnan, R., and Ehrlicher, A. (2007). The forces behind cell movement. Int J Biol Sci *3*, 303-317.

Antoku, S., and Mayer, B.J. (2009). Distinct roles for Crk adaptor isoforms in actin reorganization induced by extracellular signals. J Cell Sci *122*, 4228-4238.

Antoku, S., Saksela, K., Rivera, G.M., and Mayer, B.J. (2008). A crucial role in cell spreading for the interaction of Abl PxxP motifs with Crk and Nck adaptors. J Cell Sci *121*, 3071-3082.

Birge, R.B., Kalodimos, C., Inagaki, F., and Tanaka, S. (2009). Crk and CrkL adaptor proteins: networks for physiological and pathological signaling. Cell Commun Signal *7*, 13.

Boyle, S.N., and Koleske, A.J. (2007). Dissecting kinase signaling pathways. Drug Discov Today *12*, 717-724.

Eckes, B., Kessler, D., Aumailley, M., and Krieg, T. (1999). Interactions of fibroblasts with the extracellular matrix: implications for the understanding of fibrosis. Springer Semin Immunopathol *21*, 415-429.

Genna, A., Lapetina, S., Lukic, N., Twafra, S., Meirson, T., Sharma, V.P., Condeelis, J.S., and Gil-Henn, H. (2018). Pyk2 and FAK differentially regulate invadopodia formation and function in breast cancer cells. J Cell Biol *217*, 375-395.

Gil-Henn, H., Destaing, O., Sims, N.A., Aoki, K., Alles, N., Neff, L., Sanjay, A., Bruzzaniti, A., De Camilli, P., Baron, R., and Schlessinger, J. (2007). Defective microtubule-dependent podosome organization in osteoclasts leads to increased bone density in Pyk2(-/-) mice. J Cell Biol *178*, 1053-1064.

Gurtner, G.C., Werner, S., Barrandon, Y., and Longaker, M.T. (2008). Wound repair and regeneration. Nature *453*, 314-321.

Hinz, B., Alt, W., Johnen, C., Herzog, V., and Kaiser, H.W. (1999). Quantifying lamella dynamics of cultured cells by SACED, a new computer-assisted motion analysis. Exp Cell Res *251*, 234-243.

Ilic, D., Furuta, Y., Kanazawa, S., Takeda, N., Sobue, K., Nakatsuji, N., Nomura, S., Fujimoto, J., Okada, M., and Yamamoto, T. (1995). Reduced cell motility and enhanced focal adhesion contact formation in cells from FAK-deficient mice. Nature *377*, 539-544.

Klingbeil, C.K., Hauck, C.R., Hsia, D.A., Jones, K.C., Reider, S.R., and Schlaepfer, D.D. (2001). Targeting Pyk2 to beta 1-integrin-containing focal contacts rescues fibronectin-stimulated signaling and haptotactic motility defects of focal adhesion kinase-null cells. J Cell Biol *152*, 97-110.

Koppel, A.C., Kiss, A., Hindes, A., Burns, C.J., Marmer, B.L., Goldberg, G., Blumenberg, M., and Efimova, T. (2014). Delayed skin wound repair in proline-rich protein tyrosine kinase 2 knockout mice. Am J Physiol Cell Physiol *306*, C899-909.

Kurosaka, S., and Kashina, A. (2008). Cell biology of embryonic migration. Birth Defects Res C Embryo Today *84*, 102-122.

Lachmann, A., Schilder, B.M., Wojciechowicz, M.L., Torre, D., Kuleshov, M.V., Keenan, A.B., and Ma'ayan, A. (2019). Geneshot: search engine for ranking genes from arbitrary text queries. Nucleic Acids Res *47*, W571-W577.

Lapetina, S., and Gil-Henn, H. (2017). A guide to simple, direct, and quantitative in vitro binding assays. J Biol Methods *4*, e62.

Lapetina, S., Mader, C.C., Machida, K., Mayer, B.J., and Koleske, A.J. (2009). Arg interacts with cortactin to promote adhesion-dependent cell edge protrusion. J Cell Biol *185*, 503-519.

Lim, Y., Lim, S.T., Tomar, A., Gardel, M., Bernard-Trifilo, J.A., Chen, X.L., Uryu, S.A., Canete-Soler, R., Zhai, J., Lin, H., Schlaepfer, W.W., Nalbant, P., Bokoch, G., Ilic, D., Waterman-Storer, C., and Schlaepfer, D.D. (2008). PyK2 and FAK connections to p190Rho guanine nucleotide exchange factor regulate RhoA activity, focal adhesion formation, and cell motility. J Cell Biol *180*, 187-203.

Litvak, V., Tian, D., Shaul, Y.D., and Lev, S. (2000). Targeting of PYK2 to focal adhesions as a cellular mechanism for convergence between integrins and G protein-coupled receptor signaling cascades. J Biol Chem *275*, 32736-32746.

Martin, P. (1997). Wound healing--aiming for perfect skin regeneration. Science *276*, 75-81.

Miller, M.M., Lapetina, S., MacGrath, S.M., Sfakianos, M.K., Pollard, T.D., and Koleske, A.J. (2010). Regulation of actin polymerization and adhesion-dependent cell edge protrusion by the Abl-related gene (Arg) tyrosine kinase and N-WASp. Biochemistry *49*, 2227-2234.

Okigaki, M., Davis, C., Falasca, M., Harroch, S., Felsenfeld, D.P., Sheetz, M.P., and Schlessinger, J. (2003). Pyk2 regulates multiple signaling events crucial for macrophage morphology and migration. Proc Natl Acad Sci U S A *100*, 10740-10745.

Park, T.J., and Curran, T. (2014). Essential roles of Crk and CrkL in fibroblast structure and motility. Oncogene *33*, 5121-5132.

Parsons, J.T., Horwitz, A.R., and Schwartz, M.A. (2010). Cell adhesion: integrating cytoskeletal dynamics and cellular tension. Nat Rev Mol Cell Biol *11*, 633-643.

Roa-Espitia, A.L., Hernandez-Rendon, E.R., Baltierrez-Hoyos, R., Munoz-Gotera, R.J., Cote-Velez, A., Jimenez, I., Gonzalez-Marquez, H., and Hernandez-Gonzalez, E.O. (2016). Focal adhesion kinase is required for actin polymerization and remodeling of the cytoskeleton during sperm capacitation. Biol Open *5*, 1189-1199.

Shannon, P., Markiel, A., Ozier, O., Baliga, N.S., Wang, J.T., Ramage, D., Amin, N., Schwikowski, B., and Ideker, T. (2003). Cytoscape: a software environment for integrated models of biomolecular interaction networks. Genome Res *13*, 2498-2504.

Sieg, D.J., Ilic, D., Jones, K.C., Damsky, C.H., Hunter, T., and Schlaepfer, D.D. (1998). Pyk2 and Src-family protein-tyrosine kinases compensate for the loss of FAK in fibronectin-stimulated signaling events but Pyk2 does not fully function to enhance FAK- cell migration. EMBO J *17*, 5933-5947.

Tomar, A., Lim, S.T., Lim, Y., and Schlaepfer, D.D. (2009). A FAK-p120RasGAP-p190RhoGAP complex regulates polarity in migrating cells. J Cell Sci *122*, 1852-1862.

Vuori, K., Hirai, H., Aizawa, S., and Ruoslahti, E. (1996). Introduction of p130cas signaling complex formation upon integrin-mediated cell adhesion: a role for Src family kinases. Mol Cell Biol *16*, 2606-2613.

Figure 1

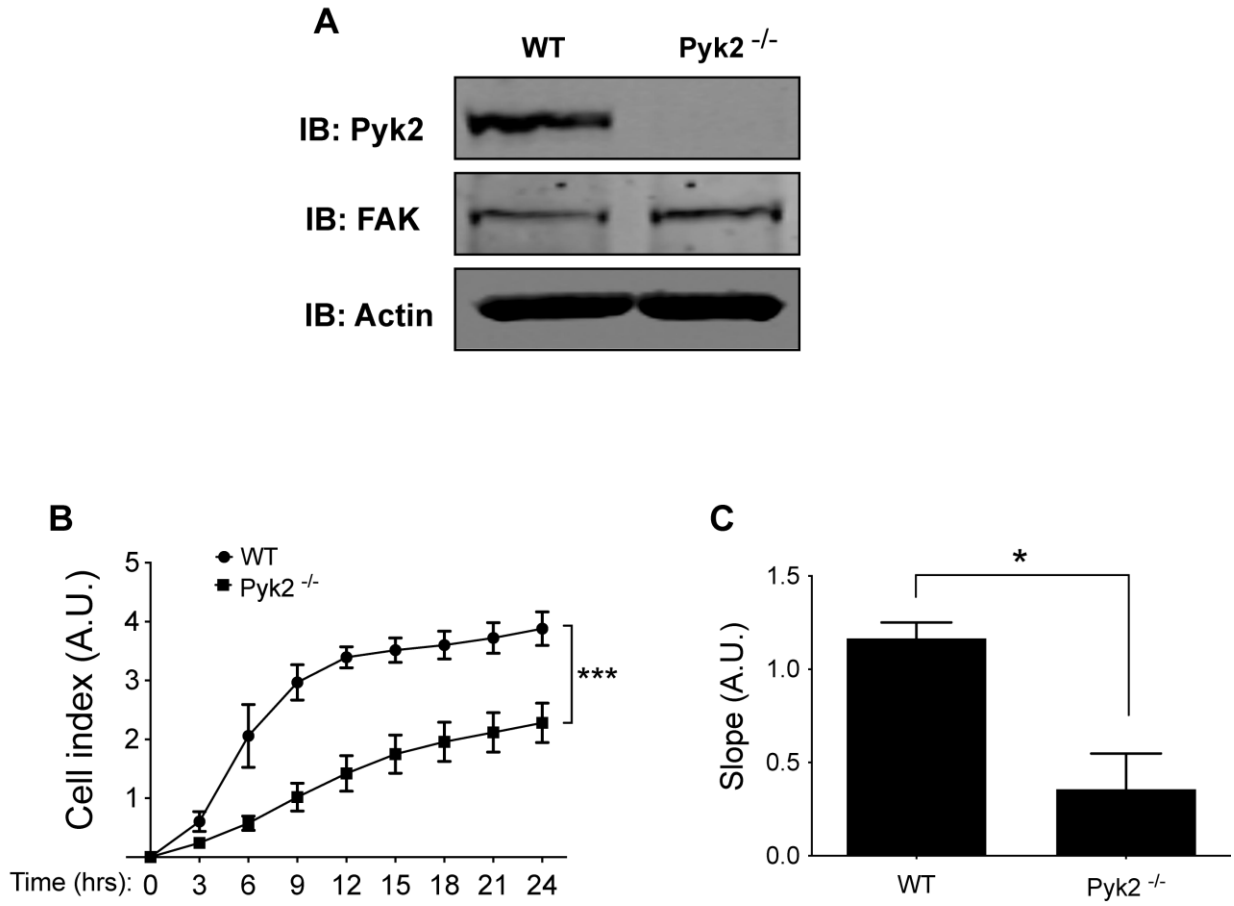

Figure 1. Pyk2$^{-/-}$ MEFs demonstrate reduced chemotactic migration. (A) Western blot analysis of whole cell lysates of WT and Pyk2$^{-/-}$ MEFs. Blots were probed for Pyk2, FAK, and actin as a loading control. **(B)** Analysis of cell invasion of WT and Pyk2$^{-/-}$ MEFs measured by xCELLigence, presented as cell index (arbitrary units) as a function of time. *** $P \leq 0.001$, $F = 35.5$ by two-way ANOVA followed by Dunnett's posthoc test, representing comparison between WT and Pyk2$^{-/-}$ through time. **(C)** Slopes of chemotactic migration graphs calculated as 1/hr. * $P \leq 0.05$ by Student's *t*-test. n = 8 wells from three independent experiments.

Figure 2

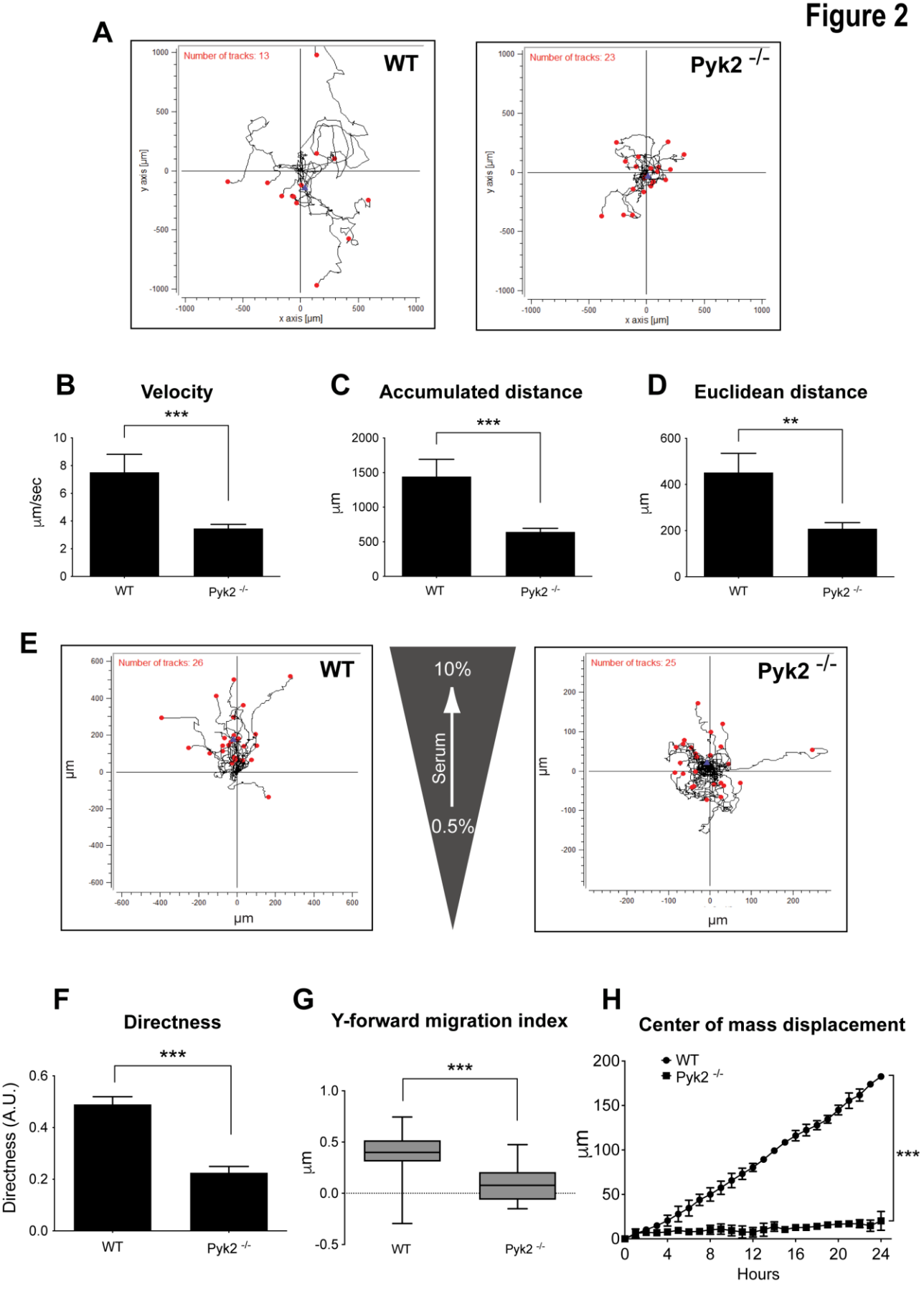

Figure 2. Knockout of Pyk2 significantly reduces random and directed single cell motility.

(A) Representative trajectory plots of WT (left) and Pyk2$^{-/-}$ (right) MEFs from a single cell random migration experiment. **(B-D)** Quantification of velocity (B), accumulated distance (C), and Euclidean distance (D), from single cell random migration experiments. ** $P \leq 0.05$, *** $P \leq 0.001$ by Student's *t* test. n = 13 cells (WT), n = 23 cells (Pyk2$^{-/-}$) from three independent experiments. **(E)** Representative trajectory plots of WT (left) and Pyk2$^{-/-}$ (right) MEFs from a directed cell motility experiment. The direction of FBS gradient (from 0.5% to 10%) is shown. **(F)** Quantification of directness, expressed in arbitrary units (A.U.). **(G)** Quantification of Y-forward migration index. *** $P \leq 0.001$ by Student's *t*-test. **(H)** Center of mass displacement. *** $P \leq 0.001$, $F = 54.65$ by two-way ANOVA followed by Dunnett's posthoc test, representing a comparison of the center of mass displacement between WT and Pyk2$^{-/-}$. n = 26 cells (WT), n = 25 cells (Pyk2$^{-/-}$) from three independent experiments.

Figure 3

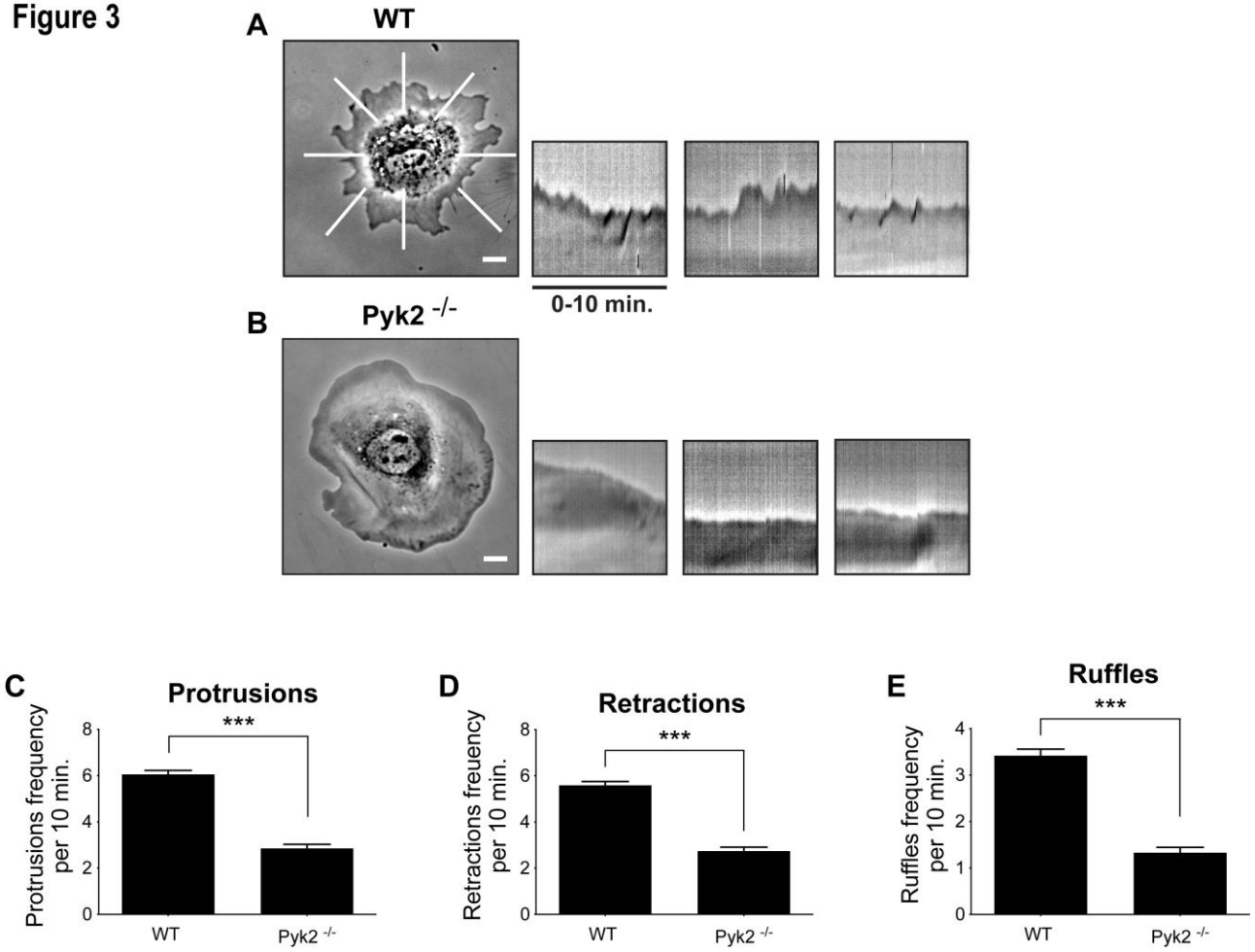

Figure 3. Pyk2$^{-/-}$ MEFs show reduced cell-edge protrusion dynamics. (A-B) Representative frames from 10 minutes time-lapse videos of WT (A) and Pyk2$^{-/-}$ (B) cells plated on fibronectin. For kymography analysis, a radial grid of eight lines was placed over the phase images as shown in A, and and kymographs were constructed for each of the indicated lines. Three representative kymographs for each cell are presented. Scale bar, 20 μm. **(C-E)** Quantification of the number of protrusions (C), retractions (D), and ruffles (E) per 10 minutes videos. *** $P \leq 0.001$ by Student's *t*-test. n = 171 cells (WT), n = 179 cells (Pyk2$^{-/-}$) from three independent experiments.

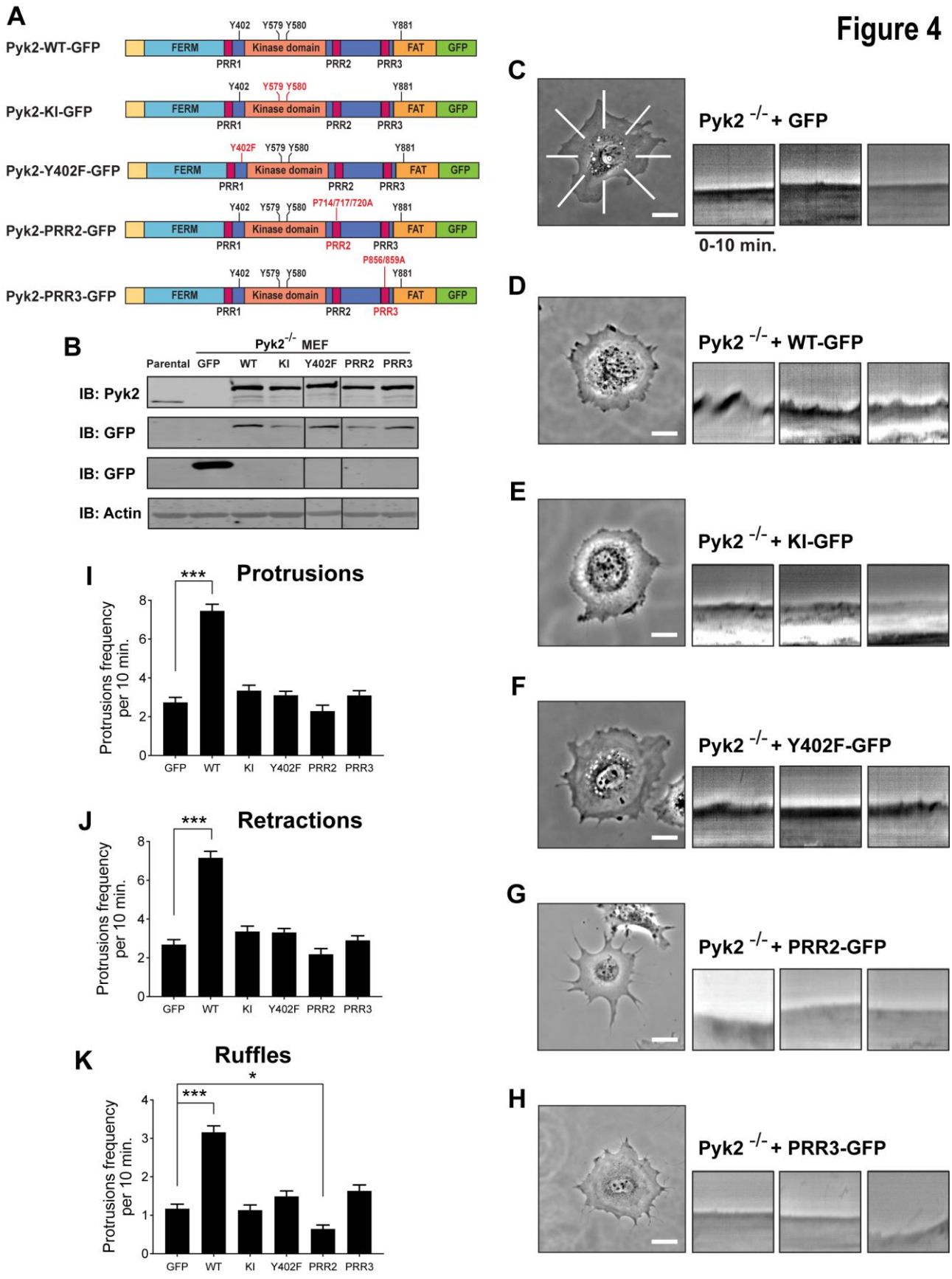

Figure 4. Regulation of cell-edge protrusion dynamics in fibroblasts depends on both the kinase and binding activities of Pyk2. (A) Graphical representation of GFP-tagged Pyk2 constructs used for re-expression in Pyk2$^{-/-}$ MEFs for protrusion assay analysis: Pyk2-WT-GFP,

Pyk2-Y402F-GFP, Pyk2-KI-GFP, Pyk2-PRR2-GFP, and Pyk2-PRR3-GFP. The specific mutations in each construct are described in Materials and Methods. **(B)** Western blot analysis of whole cell lysates of $Pyk2^{-/-}$ MEFs stably re-expressing GFP, WT-Pyk2-GFP, or Pyk2 mutants. **(C-H)** Representative images and kymographs from 10 minutes time-lapse videos of $Pyk2^{-/-}$ MEFs re-expressing WT or mutant Pyk2 forms plated on fibronectin as above. Kymographs were generated as described in Figure 4. Scale bar, 20 μm. **(I-K)** Quantification of the number of protrusions (H), retractions (I), and ruffles (J) per 10 minutes videos. * $P \leq 0.05$, *** $P \leq 0.001$, $F = 49.05$ (H), $F = 45.57$ (I), $F = 39.39$ (J), by one-way ANOVA followed by Dunnett's posthoc test. n = 14 cells ($Pyk2^{-/-}$ + GFP), n = 16 cells ($Pyk2^{-/-}$ + Pyk2-WT), n = 13 cells ($Pyk2^{-/-}$ + Pyk2 Y402F), n = 15 cells ($Pyk2^{-/-}$ + Pyk2-KI), n = 13 cells ($Pyk2^{-/-}$ + Pyk2-PRR2), n = 15 cells ($Pyk2^{-/-}$ + Pyk2-PRR3) from three independent experiments.

Figure 5

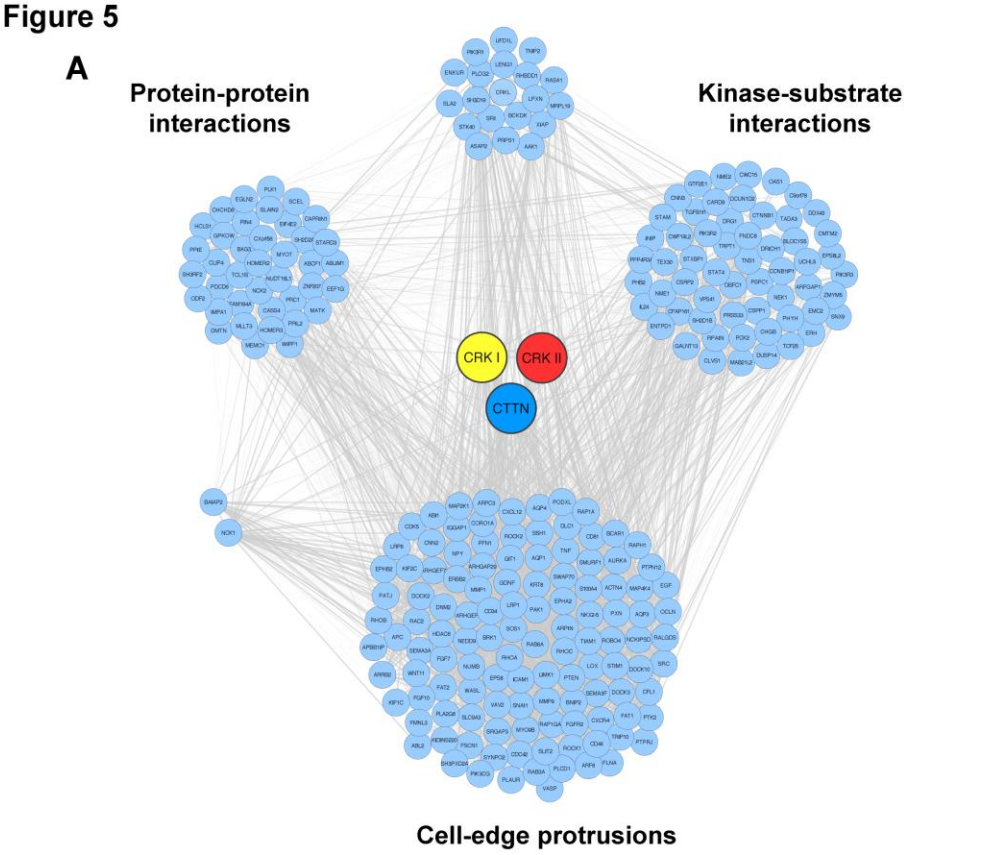

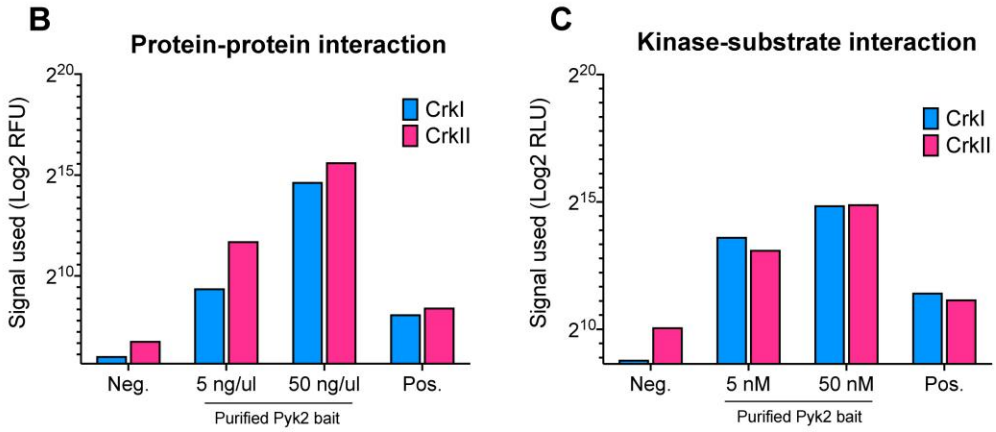

Figure 5. CrkI and CrkII are potential substrates and interactors of Pyk2. (A) Overlap of protein-protein interaction protein list (PPI) with kinase-substrate interaction protein list (KSI) and with cell-edge protrusions list which was obtained by literature mining using Geneshot. The lists of proteins were overlaid using Cytoscape, and the combined list of common nodes was used to build a physical and functional association network in STRING (gray lines). **(B)** Protein-protein interaction background-subtracted pixel intensity values (signal used) of CrkI (blue) and CrkII (pink) in two concentrations of Pyk2 that were used for screening, compared with the positive and negative controls. Z-score (50 ng/ul) = 7.41 (CrkI), 14.84 (CrkII); CI p-value (50ng/µl) = 2.77×10^{-5} (CrkI), 1.02×10^{-4} (CrkII). **(C)** Kinase-substrate interaction values (signal used) of CrkI and CrkII in two concentrations of Pyk2 that were used for screening, compared with the positive and negative controls. Z-score (50 nM) = 3.55 (CrkI), 3.97 (CrkII); CI p-value (50ng/µl) = 4.7×10^{-3} (CrkI), 3.4×10^{-3} (CrkII).

Figure 6

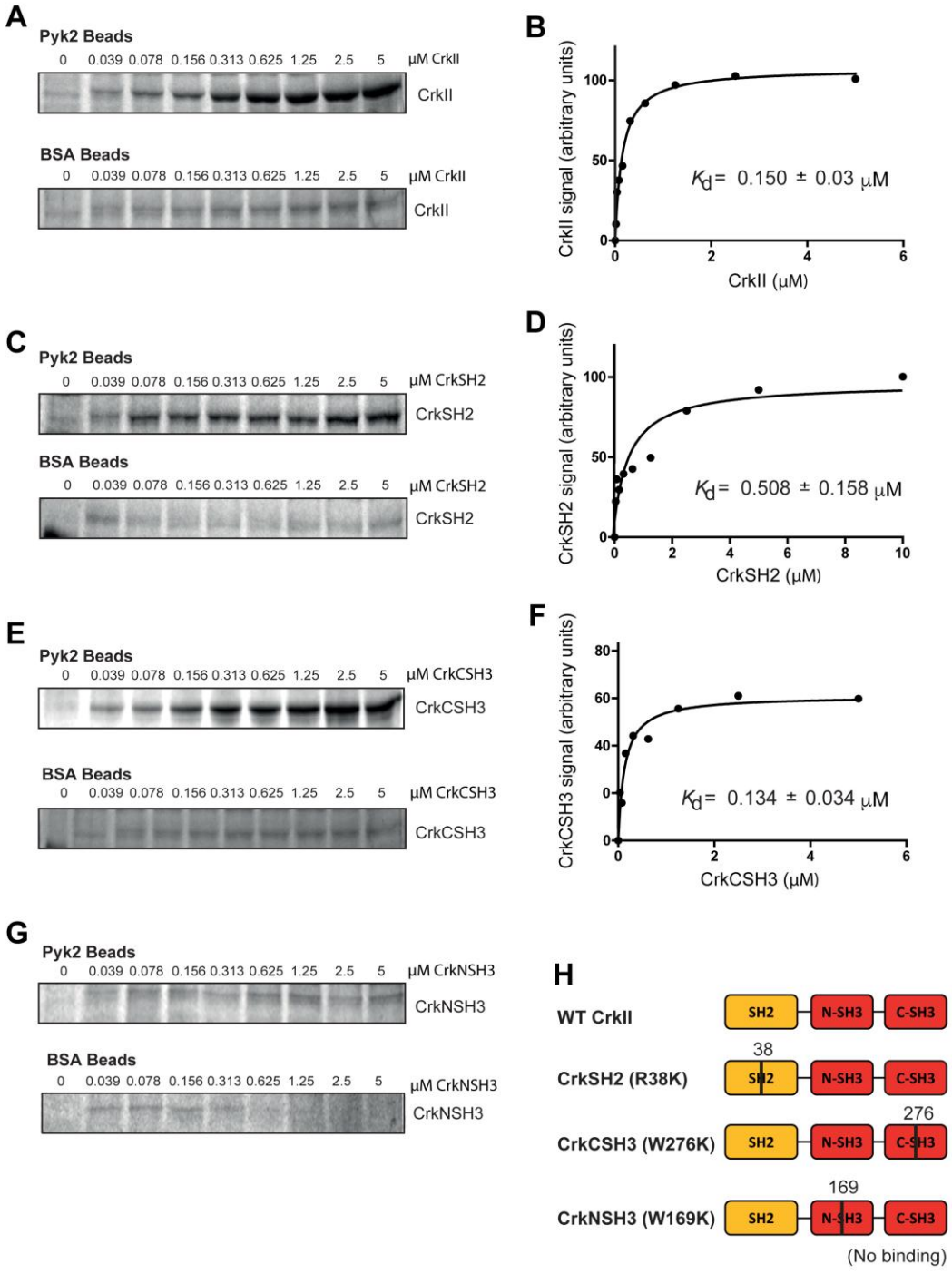

Figure 6. CrkII is a direct interactor of Pyk2. (A-G) Increasing concentrations (0-5 µM) of recombinant WT GST-CrkII (A-B), GST-CrkSH2 (a mutation at the SH2 domain; (C-D), GST-CrkCSH3 (a W276K mutantion at the C-terminal SH3 domain; E-F), or GST-CrkNSH3 (a mutantion at the N-terminal SH3 domain; G) were incubated with 1 mM Pyk2 covalently bound to AminoLink beads or to BSA control beads only. The amount of CrkII pulled down nonspecifically by BSA-coated AminoLink beads was deducted from CrkII pulled down by Pyk2 coated beads. n=4 independent pulldown experiments. **(H)** Graphical representation of CrkII mutants that were used in this experiment: WT-CrkII, CrkSH2 (R38K), CrkCSH3 (W276K), and CrkNSH3 (W169K). No binding was observed between Pyk2 and CrkNSH3.

Figure 7

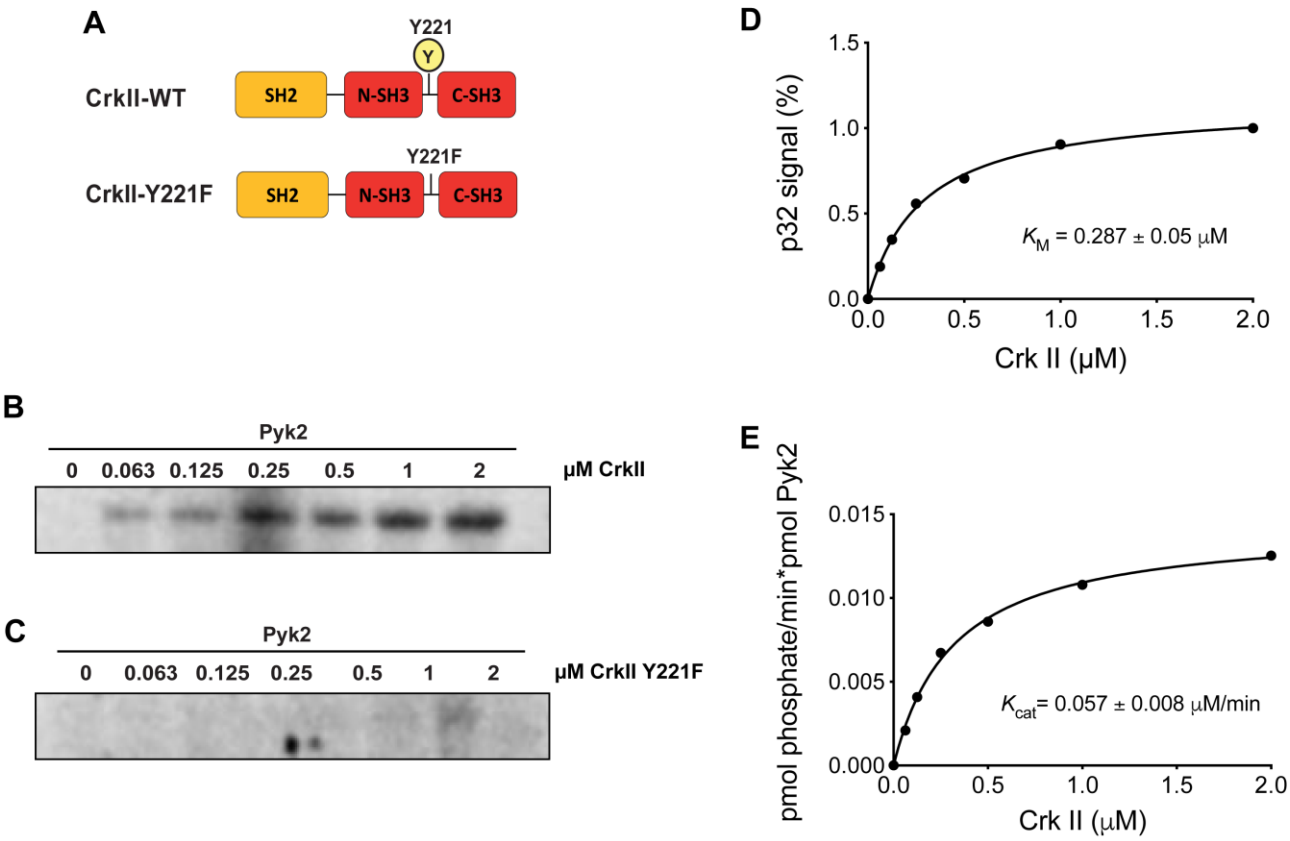

Figure 7. CrkII is a direct substrate of Pyk2. Increasing concentrations of recombinant WT GST-CrkII (I, K-L) or GST-CrkII-Y221F (tyrosine phosphorylation deficient mutant; J) were incubated with constant concentrations of Pyk2 (10 nM) in presence of γ^{32}-P-ATP. Kinase reactions were permitted to proceed for 5 minutes and then quenched by adding Laemmli sample buffer and boiling for 5 min. Reactions were run on an SDS-PAGE and exposed to a phosphoimager screen. **(A)** Graphical representation of CrkII WT and mutant used in this experiment. **(B-E)** Representative phospho-images **(B-C)** and graphs **(D-E)** from three independent experiments each. Kinetics values for WT CrkII: K_M = 0.287 ± 0.05 µM, k_{cat} = 0.057 ± 0.008 µM/min, k_{cat}/K_M = 1.092 min^{-1} $µM^{-1}$.

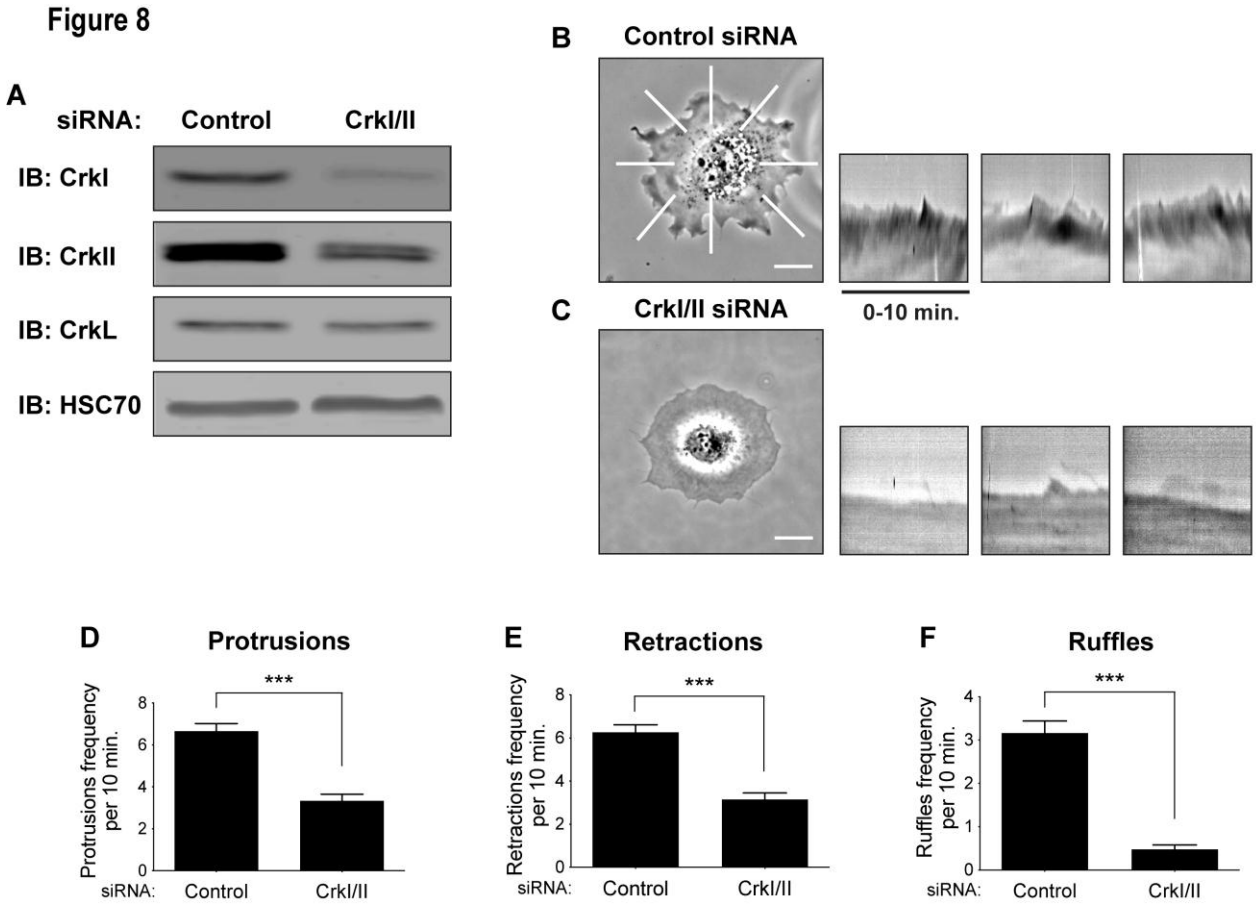

Figure 8. Knockdown of CrkII significantly reduces cell-edge protrusion dynamics.

(A) Representative immunoblot of WT MEFs transfected with control or CrkII siRNA. Blots were probed with anti-CrkII, anti-CrkL, or anti-HSC70 antibody as loading control. Note that the CrkII siRNA sequences also reduce the protein amount of CrkI, but does not affect the levels of CrkL. **(B-C)** Representative images and kymographs from 10 minutes time-lapse videos of WT MEFs transfected with control or CrkII siRNA and plated on fibronectin as above. Kymographs were generated as described in Figure 4. Scale bar, 20 μm. **(D-F)** Quantification of the number of protrusions (D), retractions (E), and ruffles (F) per 10 minutes videos. *** $P \leq 0.001$ by Student's *t* test. n = 56 cells (control siRNA), n = 48 cells (CrkII siRNA) from three independent experiments.

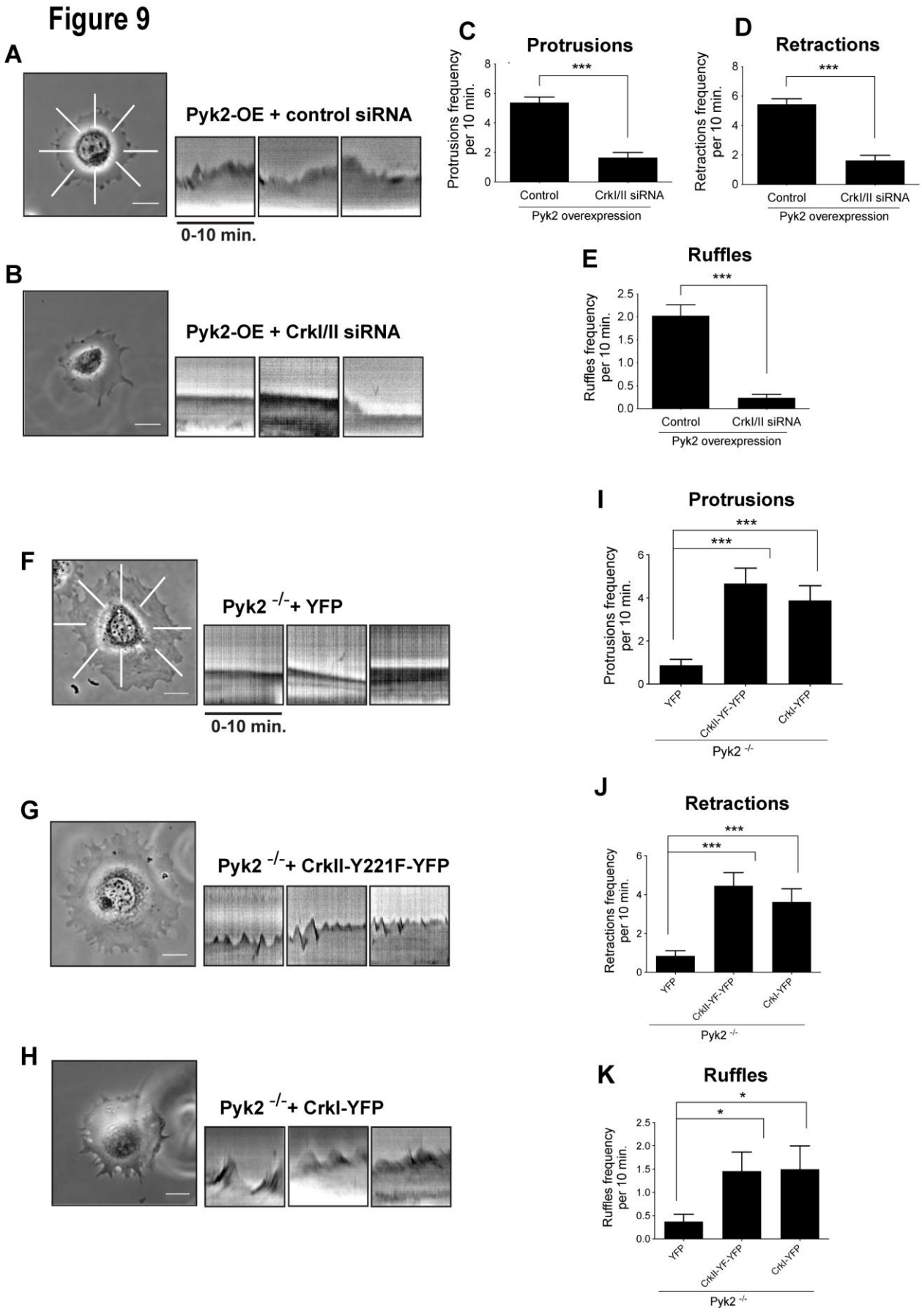

Figure 9. Pyk2 and CrkII coordinately regulate cell-edge protrusion dynamics.

(A-B) Representative images and kymographs from 10 minutes time-lapse videos of MEFs overexpressing Pyk2 and transfected with either control siRNA (Pyk2-OE + control; A) or with CrkII siRNA (Pyk2-OE + CrkII-KD; B) and plated on fibronectin as above. Kymographs were generated as described in Figure 4. Scale bar, 20 μm. **(C-E)** Quantification of the number of protrusions (C), retractions (D), and ruffles (E) per 10 minutes videos. *** $P \leq 0.001$ by Student's *t*-test. n = 38 (for Pyk2-OE + control and for Pyk2-OE + CrkII-KD). **(F-H)** Representative images and kymographs from 10 minutes time-lapse videos of $Pyk2^{-/-}$ MEFs overexpressing YFP (F), CrkII-Y221F-YFP (G), or CrkI-YFP (H) and plated on fibronectin as above. Kymographs were generated as described in Figure 4. Scale bar, 20 μm. **(I-K)** Quantification of the number of protrusions (I), retractions (J), and ruffles (K) per 10 minutes videos. * $P \leq 0.05$, *** $P \leq 0.001$, $F = 14.54$ (I), $F = 13.97$ (J), $F = 4.935$ (K), by one-way ANOVA followed by Dunnett's posthoc test. n = 32 ($Pyk2^{-/-}$ + YFP), n = 24 ($Pyk2^{-/-}$ + CrkII-Y221F-GFP), n = 17 ($Pyk2^{-/-}$ + CrkI-YFP) from three independent experiments.

Figure 10

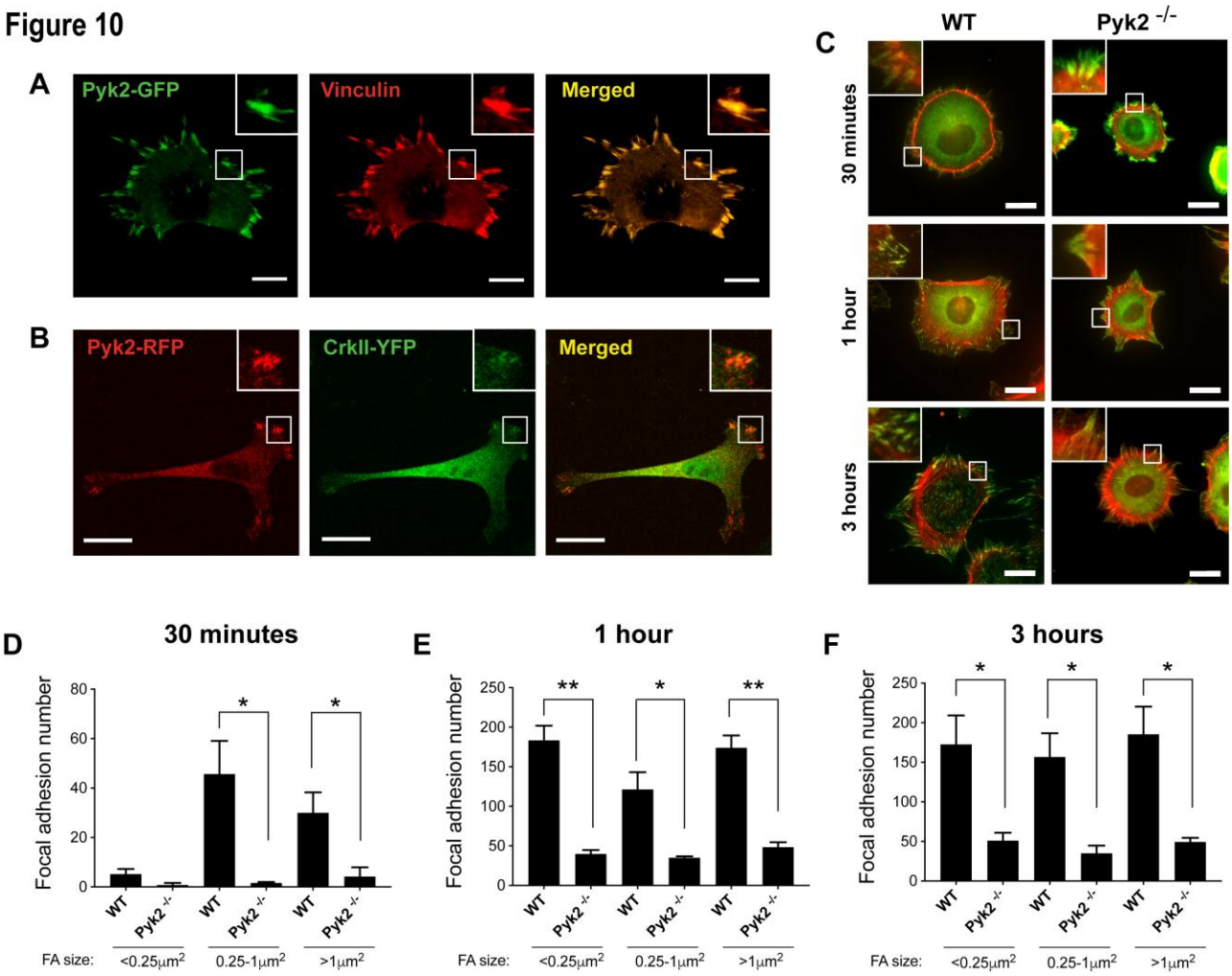

Figure 10. Pyk2 co-localizes with CrkII to focal adhesions and regulates their number and size. (A) Pyk2$^{-/-}$ MEF expressing Pyk2-WT-GFP (green) were plated on fibronectin-coated coverslips, fixed, and labeled for vinculin as a focal adhesion marker (red). Insets depict magnification of boxed areas showing cell-edge focal adhesions. Scale bar, 20 μm. **(B)** Pyk2$^{-/-}$ MEF co-expressing Pyk2-WT-RFP (red) and CrkII-YFP (green) were plated on fibronectin-coated coverslips and fixed. Insets depict magnification of boxed areas showing localization to cell-edge focal adhesions. Scale bar, 20 μm. **(C)** WT and Pyk2$^{-/-}$ MEF were plated on fibronectin-coated coverslips, fixed 30 minutes, 1 hour, or 3 hours after spreading and labeled for vinculin (green) and actin (red). Insets depict magnification of boxed areas showing focal adhesions. Scale bar, 20 μm. **(D-F)** Quantification of the number of focal adhesions which are smaller than 0.25 μm^2, between 0.25-1 μm^2, and larger than 1μm^2 at 30 minutes **(D)**, 1 hour **(E)**, and 3 hours **(F)** following plating on fibronectin. ** $P \leq 0.05$, *** $P \leq 0.001$ by Student's *t* test. n < 300 focal adhesions from each WT or Pyk2$^{-/-}$ from three independent experiments.

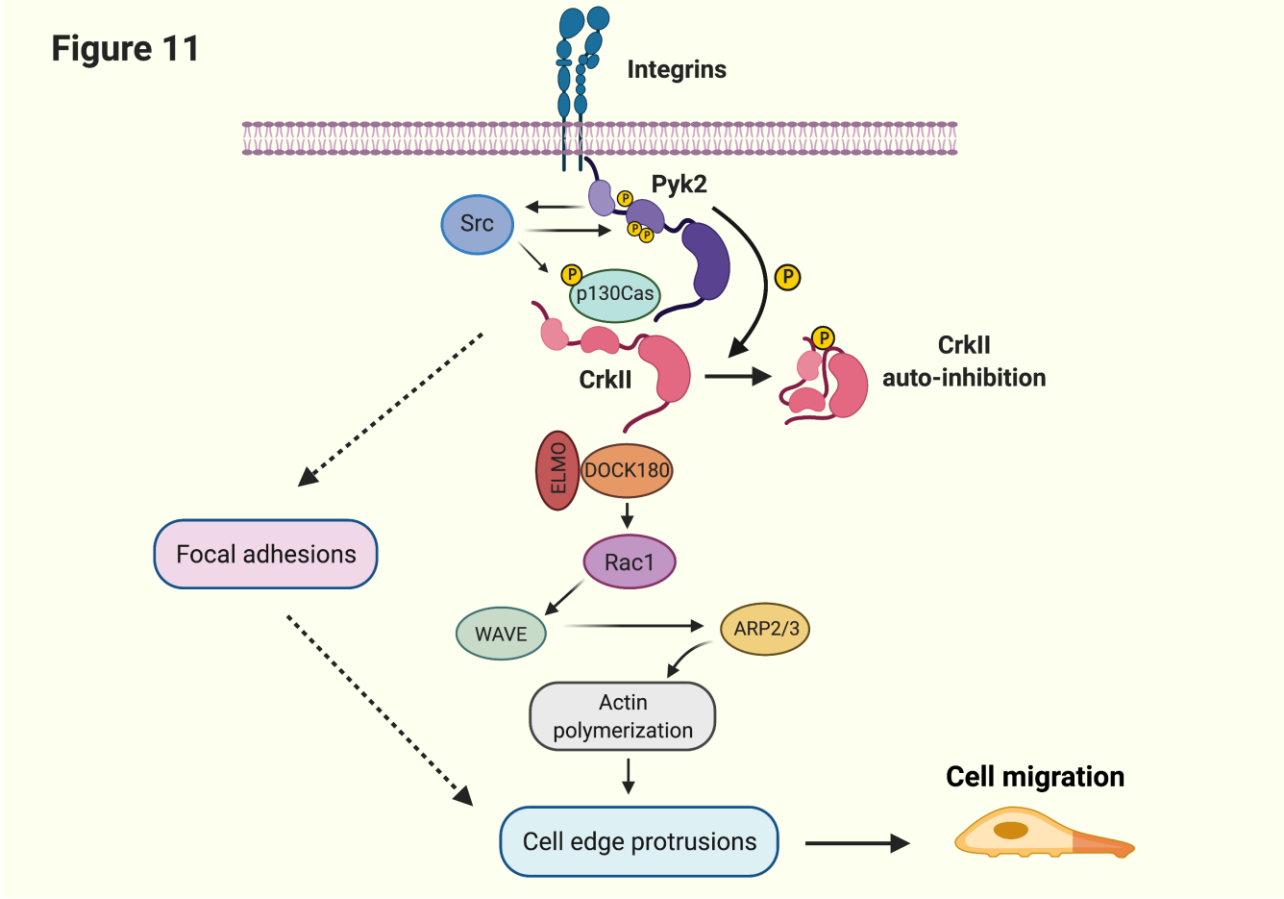

Figure 11. Pyk2 regulates cell-edge protrusion dynamics by direct and indirect interactions with Crk. Integrin binding stimulates Pyk2 autophosphorylation followed by recruitment and activation of Src, which leads to complete activation of Pyk2 by phosphorylating its kinase activation loop tyrosines. Activated Src further phosphorylates p130Cas, which recruits Crk and induces downstream signaling via DOCK180/ELMO-Rac1-WAVE-Arp2/3, leading to actin polymerization and consequent cell-edge protrusions. Activated Pyk2 can also bind directly to Crk and phosphorylate it on tyrosine 221, which leads to its autoinhibition and to downregulation of Crk-mediated signaling. Pyk2, presumably by directly interacting with CrkII, also regulates the formation and turnover of focal adhesions, which stabilize these actin-polymerization dependent protrusions at the cell-edge. These two Pyk2-mediated processes control the dynamics of protrusions at the cell-edge and consequent fibroblast motility.